physica status solidi rrl
www.pss-rapid.com

Current Status of Hollow Cathode Gas Flow Sputtering for Advanced TCOs

Bernd Szyszka, Sri Hari Bharath Vinoth Kumar, Ruslan Muydinov, Manuel Hartig, Nivin Alktash, Fangfang Huo, Bertwin Bilgrim Otto Seibertz, Nisarg Nijanandi, Kai Ortner, Dennis Barton, and Steve Albrecht*

Herein, the recent findings on hollow cathode gas flow sputtering (GFS) of transparent conductive oxides (TCO) films are reviewed. The GFS is a unique deposition technique that offers extraordinary process conditions for thin-film growth. The GFS core element is a hollow cathode discharge operating in the mbar pressure range. The sputtered atoms are transported by means of forced convection. These key features allow for unique deposition conditions: i) GFS is a remote process where reactive gas does not interact with the sputtered target surface. This allows for high process stability at any reactive gas partial pressure, opening up even the pathway for combined physical vapor deposition (PVD) and plasma enhanced chemical vapor deposition (PECVD) synthesis. ii) The GFS plasma delivers high plasma density in the order of 10^{12} cm^{-3} at the substrate position. When bipolar pulsing is applied to the hollow cathode, plasma-activated growth can be obtained even for insulating substrates. iii) Doped films can be produced in an elegant way when the target is composed from ring segments to adjust the specified doping level. In this article, the focus is on the process development using direct simulation Monte Carlo modeling of the deposition process and on the optimization of bipolar pulsing. Follow on this, two application cases are introduced: i) synthesis of p-type NiO_x and Cu-doped and NiO_x-doped films for application as hole conductor in perovskite solar cells where improved device stability is achieved compared to surface assembled monolayers which are state of the art and ii) synthesis of ZnO_xN_y films with the perspective for usage as semiconductive films in thin-film transistors.

1. Introduction

While the history of transparent conductive oxides dates back to more than 100 years from now, it is the intense development of advanced optoelectronic products that raised substantial research on materials and deposition processes in this area. In many cases, these transparent conductive oxides (TCO) films are used as contact layers to sensitive semiconductive films, e.g., in heterojunction solar cells with intrinsic thin film (HIT cells) and light-emitting diodes. Here, any damage induced by fast particles must be prevented to ensure the ultimate device performance. Furthermore, issues such as the proper band alignment must be maintained, which requires precise control of defect states and doping levels.

Beyond this level of TCO application, we have to address the subject of active semiconductive oxides where the electronic properties of the films are subject to modulation, e.g., by means of the electric field in a thin film transistors (TFT) structure and furthermore, we need to consider p-type materials, e.g., for hole extraction in thin-film perovskite solar cells (PSCs). Within this article, we address these items focussing on p-type conductive NiO_x and doped NiO_x films as hole transport layers (HTLs) for PSCs and on semiconductive

B. Szyszka, S. H. B. Vinoth Kumar, R. Muydinov, M. Hartig, N. Alktash, F. Huo, B. B. O. Seibertz, N. Nijanandi
Chair Technology of Thin Film Device TFD
TU Berlin
Einsteinufer 25, Office HFT 5-2, 10587 Berlin, Germany
E-mail: bernd.szyszka@tu-berlin.de

The ORCID identification number(s) for the author(s) of this article can be found under https://doi.org/10.1002/pssr.202500080.

DOI: 10.1002/pssr.202500080

K. Ortner, D. Barton
Fraunhofer Institute for Surface Engineering and Thin Films IST
Riedenkamp 2, 38108 Braunschweig, Germany

S. Albrecht
Perowskit Tandemsolarzellen
Helmholtz-Zentrum Berlin für Materialien und Energie
Hahn-Meitner-Platz 1, Berlin, Germany 14109

zinc-oxynitride films for TFTs taking the special properties of the hollow cathode gas flow sputter (GFS) process into account.

Looking back in history, the deposition of thin films by sputtering has been an enabling technology for a large variety of technical applications such as large area glass coating for energy efficiency in architectural and automotive applications, for solar absorbers, solar cells, and flat panel displays, for microelectronics, and hard coatings for tools and parts and numerous further areas.[1] Early applications have been realized with planar targets sputtered at high voltage of approx. 2–3 kV in the pressure range of 10^{-1} mbar.[2] Due to the invention of the magnetically confined discharge in the so-called magnetron geometry, the voltage could be decreased towards approx. 100–500 V to be applied at the cathode. In parallel to this, a decrease in discharge pressure toward the 10^{-3} mbar range has been realized.[3] Sputtering under such conditions allows for higher discharge current and thus increased depostion rate plus advantages in thin film deposition since the energy of sputtered particles contributes to the surface diffusion on the substrate and thus to the formation of more dense films. Despite these advantages, the magnetron sputtering reveals limitations, mainly due to the unwanted reaction of reactive gas with the cathode surfaces, which requires complex techniques for process control and stabilization,[4] but also due to the fact that high energetic species still exist in form of fast reactive gas ions and reflected sputter gas neutrals, which induce damage to the growing film. Increasing pressure allows for a thermalization of these fast species where the initial energy exceeds 100 eV, but due to the energy dependence of the scattering cross sections, this is even more severe for the low energetic sputtered particles.[5] Common understanding about these effects has been achieved already in the 1980s, and intense research was stimulated toward low voltage magnetron sputtering, pulse magnetron sputtering, rotatable magnetron sputtering, moving magnet sputtering, and meta mode sputtering, where sputter zone and reaction zone have been separated by means of rotating substrates.[1]

During the 1980s, a novel concept has been developed to circumvent the limitations outlined above: It is based on the utilization of two principles: First, the usage of the hollow cathode effect to generate the plasma for cathode sputtering and second the transport of the sputtered particles toward the substrate by means of forced convection.[6,7] From practical point of view, several advantages compared to magnetron sputtering have been described: i) the equipment for mbar range of operation is much easier to build compared to costly high vacuum equipment necessary for magnetron sputtering, ii) the target utilization is in the order of 90%, since no magnets are used, iii) the deposition rate is high, even for compound layers, since the target surface is not covered with reaction products, and iv) the GFS operates under steady-state conditions, so process control does not require fast closed loop control loops, like in reactive magnetron sputtering of compound films.[4]

Consequently, substantial research on functional oxides for electrical and optical applications has been undertaken in the last couple of years, taking advantage of the special process conditions available in GFS. Well-known applications such as indium tin oxide (ITO) sputtering with high target utilization[8] and ZnO:Al sputtering[9] have been demonstrated by GFS, p-type oxides such as Delafossite $CuCrO_2$ and $CuAlO_2$ have been manufactured,[10] and photocatalytic TiO_2[11] and WO_3-based[12] coatings have been developed.

On the other hand, some difficulties have been observed in the last few decades, which have hindered the successful industrialization of GFS technology. For example, the dark space shielding must be much thinner compared to magnetron sputtering and thus, a risk of unwanted parasitic discharges is given, in particular for long linear sources.[8] By means of advanced process modelling, however, such items can be controlled. From thin-film growth perspective, however, the GFS allows for excellent abilities to tailor the growth. Issues such as physical vapor deposition (PVD)/plasma enhanced chemical vapor deposition (PECVD) hybrid process can easily be achieved due to the high pressure. Ion-assisted growth is feasible due to the high plasma density at the substrate, but also a magnetic field can be applied to shield the substrate, for example, for device quality a-Si:H sputtering.[13] Even nanoparticles can be grown in a controlled manner.[14]

2. Experimental Section

Within the work described here, we address the usage of small-scale GFS source which consists of a target tube of 60 mm length

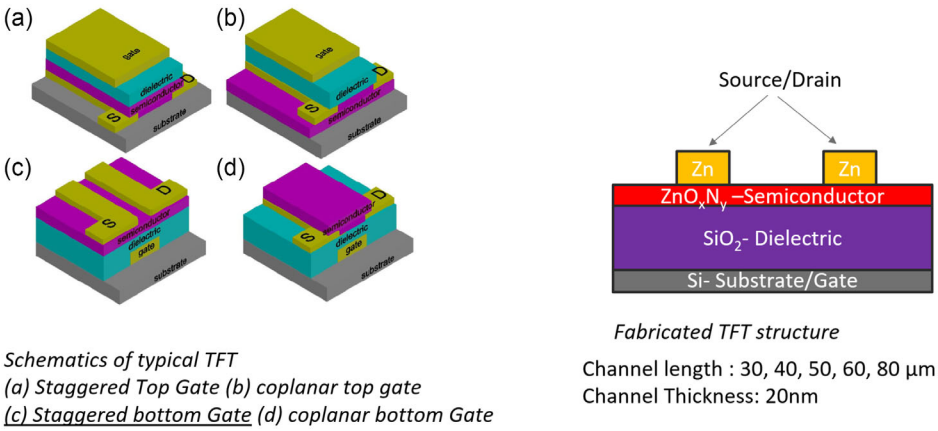

Schematics of typical TFT
(a) Staggered Top Gate (b) coplanar top gate
(c) Staggered bottom Gate (d) coplanar bottom Gate

Fabricated TFT structure
Channel length : 30, 40, 50, 60, 80 µm
Channel Thickness: 20nm

Figure 1. Layout of TFT structure (left) and TFTs realized using oxidized Si wafers (right).

and 40 mm diameter. This GFS tool is homemade and a concise overview of the tool and experimental details relevant to the research discussed in this study is provided elsewhere in Ref. [15]

To explore different hole-transporting layers (HTLs) in metal halide PSCs, the device structure employed was as follows: Glass/ITO (150 nm)/various HTLs/Perovskite (≈450 nm)/C60 (23 nm)/Bathocuproine (8 nm)/Cu (100 nm), with an active area of 16 mm^2. The perovskite layer, composed of the triple-cation formulation $Cs_{0.05}(MA_{0.17}FA_{0.83})_{0.95}Pb(I_{0.83}Br_{0.17})_3$, was prepared using a previously reported method and exhibited a bandgap of ≈1.6 eV.[16] The various GFS HTLs were benchmarked against state-of-the-art self-assembled monolayers (SAM, MeO − 2PACz: [2-(3,6-dimethoxy-9H-carbazol-9-yl)ethyl] phosphonic acid).[16] The NiO_x films were prepared by sputtering using a metallic Ni target (4 N purity, 60 mm in length, 50 mm outer diameter, and 40 mm inner diameter). NiO_x:Cu, NiO_x:Mg, NiO_x:Zn, and NiOx:Fe films were fabricated by replacing a portion of the Ni target with rings of Cu, Mg, Zn, and Fe,

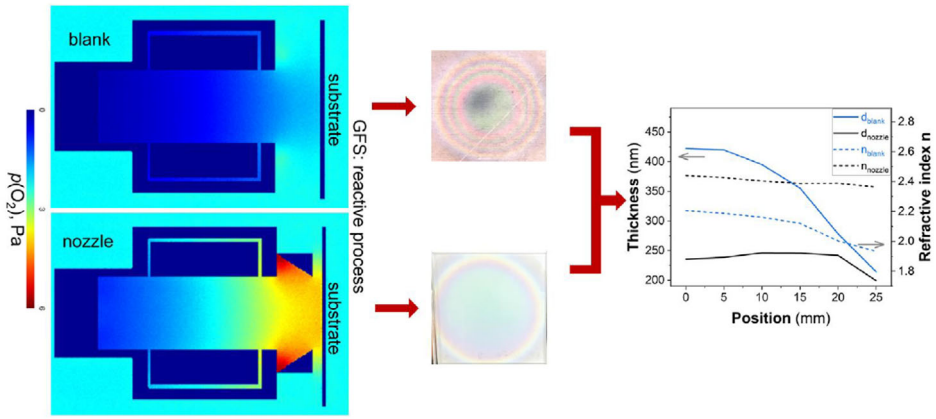

Figure 2. Left: Simulation of reactive gas partial pressure distribution at the deposition zone without (top) and with (bottom) attached nozzle. Center: Corresponding interference fringes of TiO_2 films on 50 × 50 mm^2 glass. Right: Distribution of film thickness and homogeneity obtained from ellipsometry.[17]

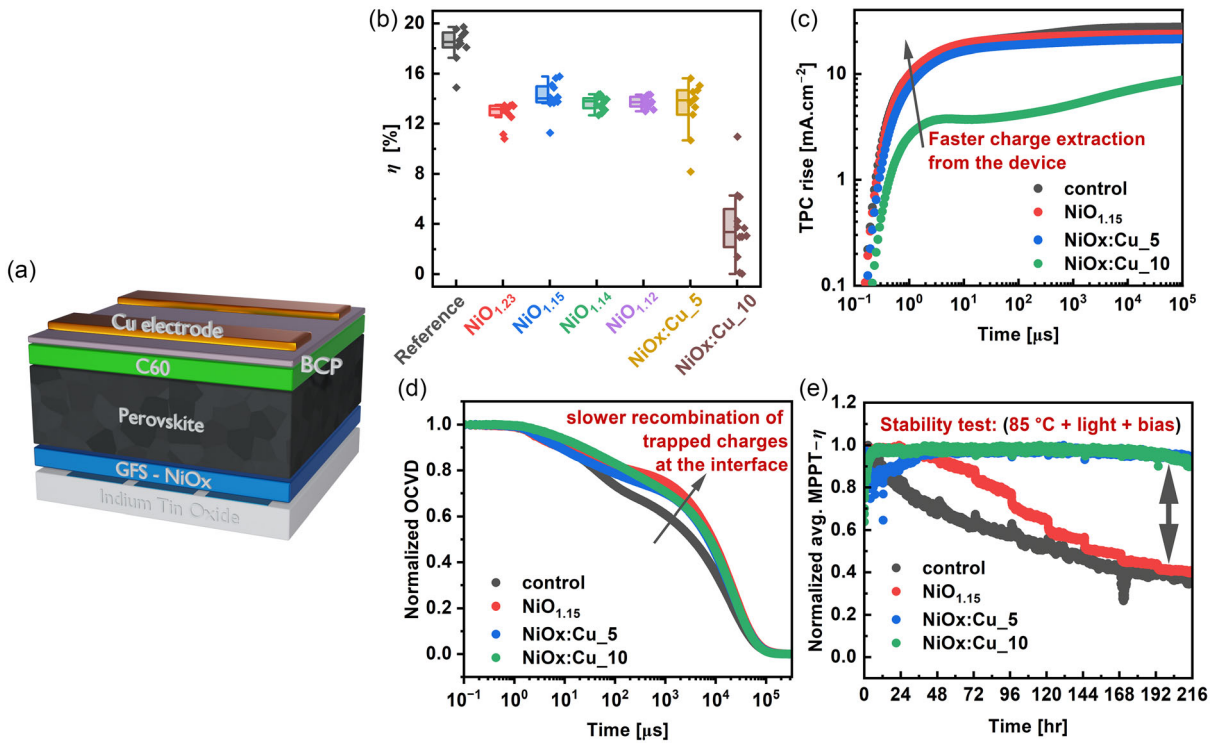

Figure 3. Results for Perovskite solar celusing a) using surface-assembled monolayers (reference) and GFS sputtered NiO_x and NiO_x:Cu as HTL.[21] b) efficiency (η) from current–voltage (J–V) measurement under AM 1.5 G illumination, c) TPC rise, d) normalized OCVD, e) Normalized averages of maximum power point tracking–η of the PSCs under the operational stability test.

respectively, each with a length of 5 mm. Unless specified otherwise, the non-Ni metallic rings used were 5 mm in length. For NiO_x:Cu films, where both 5 mm and 10 mm Cu rings were utilized, the resulting films are denoted as NiO_x:Cu_5 and NiO_x:Cu_10, respectively. The compositions of the NiO_x, NiO_x:Cu_5, and NiO_x:Cu_10 films were determined to be $NiO_{1.15}$, $Cu_{0.1}Ni_{0.9}O_{1.11}$, and $Cu_{0.15}Ni_{0.85}O_{1.0}$, respectively.[21] The properties of the other NiO_x-based films are currently under investigation.

To investigate the synthesis of semiconductive ZnO_xN_y films[22] for transparent thin-film transistors by reactive hollow cathode gas flow sputtering, we used the same gas flow sputter source as described above using a metallic Zn target (4 N purity). The reactive hollow cathode GFS is ideal for the synthesis of such complex oxynitride films since the reactive gas does not interact with the surface of the target material. Therefore, the continuous variation of film composition at the substate is possible by changing the reactive gas composition without altering the sputter process at the target surface. Our device layout is shown in **Figure 1**. Semiconductive ZnO_xN_y films with thickness of 20 nm have been deposited on oxidized wafers. Zn films deposited using a shadow mask have been used as source and drain electrodes.

3. Results

3.1. Optimization of Thin-Film Homogeneity

A key issue for the laboratory work is the ability of the device to provide homogeneous films on a reasonable dimension of the substrate, e.g., to perform X-ray reflectivity measurements which require a certain substrate area and to generate solar cells which can be tested in standard set-ups. By means of model-based process analysis, we developed an external nozzle for the source which concentrates the gas flow and which maintains a homogenous film stoichiometry and film thickness over 40 mm diameter on a $50 \times 50\,mm^2$ glass substrate (see **Figure 2**).[17]

3.2. NiO_x and NiO_x:Cu for PSCs

The efficiency and stability of metal halide PSCs depend strongly on the performance of the hole-transport layers (HTL).[18] Recently, the technology of SAM received strong interest due to their high-performance efficiencies.[19] Due to limitations of SAMs regarding stability and large-scale manufacturing, inorganic HTLs and bilayers of SAMs and inorganic layers are of

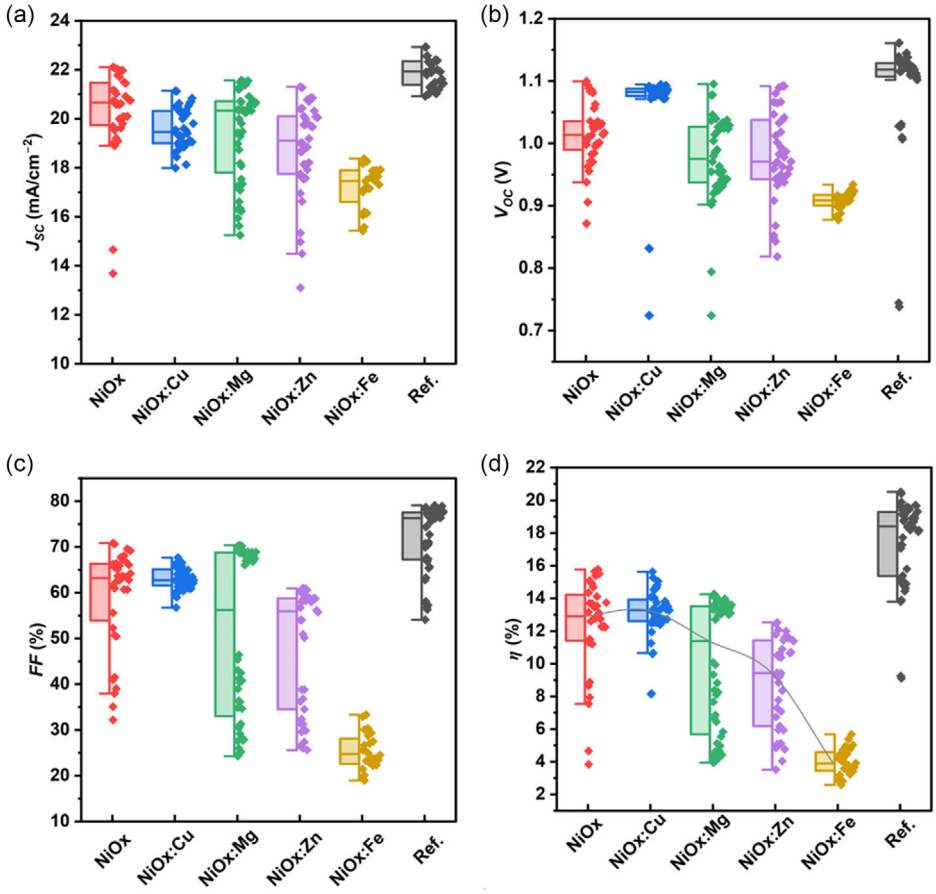

Figure 4. Results for PSCs using surface-assembled monolayers (Ref.) and GFS sputtered NiO_x as HTL. Photovoltaic parameters of the PSCs: a) short-circuit current (J_{SC}), b) open-circuit voltage (V_{OC}), c) FF, and, d) efficiency (η) from J–V measurement under AM 1.5 G illumination. The "Ref." devices are based on MeO—2PACz (SAM). The grey curve in d) is a guide to the eye. The schematic of the PSCs under investigation is shown in (a) in left part of Figure 3.

strong interest. The properties of NiO_2 films make them a strong candidate for use as a HTL in PSCs. From the viewpoint of band alignment, NiO_x-based films meet the requirements to be used as HTL for PSCs.[20] In a recent study, we investigated the usage of gas flow sputtered NiO_x and NiO_x:Cu films for this application.[21]

Our results shown in **Figure 3** reveal that SAM-based devices perform efficiency-wise slightly better compared to NiO_x and NiO_x:Cu HTLs. Furthermore, we conducted transient measurements, including transient photocurrent (TPC) and open-circuit voltage decay (OCVD), on the devices. These measurements suggest that while NiO_x HTLs can achieve a charge-extraction density comparable to SAMs, they experience interfacial charge recombination, highlighting the need for surface passivation.[21] Furthermore, strong improvements of device operational stability are reached when Cu-doping is used.

Additionally, we investigated the effects of incorporating various elements, including Cu, Mg, Zn, and Fe, into NiO_x as HTLs in PSCs. As shown in **Figure 4**, the reference devices outperformed all the NiO*x* devices in terms of performance parameters. Among the devices with non-incorporated (pure) NiOx layers, those with NiO_x:Fe experienced notable deficiencies in open-circuit voltage (V_{OC}) and fill factor, resulting in lower efficiency (η). Of the variants Cu, Mg, and Zn: Cu-incorporated NiO_x exhibited the best performance, comparable to that of pure NiO_x devices. NiO_x:Mg devices also approached the performance level of NiO_x:Cu devices, while NiO_x:Zn devices were less effective compared to both Mg- and Cu-incorporated NiO_x devices.[22]

Furthermore, **Figure 5** presents the average maximum power point tracking efficiencies (MPPT − η) of devices based on various HTLs throughout 240 h with each type showing different stability and degradation rates. The solar cells were aged in a custom-built high-throughput aging setup,[23] and the test is by the protocol ISOS-L-2I.[24] NiO_2:Cu and NiO_2:Mg devices show the best stability over time, indicating that doping NiO_2 with these elements improves the material's performance under thermal stress and illumination. Reference (SAM) and pure NiO_2 devices show the most significant degradation, with reference devices experiencing rapid initial decay and NiO_2 devices showing a more steady decline. Reference and undoped NiO_2 devices had initial efficiencies of ≈16% and 13%, respectively, which decay at the end of 240 h close to ≈9% and 4%, respectively. Similarly, the NiO_2:Cu and NiO_2:Mg devices had an initial efficiency of ≈12% and 13%, respectively, which resulted in ≈13% and 11%, respectively, at the end of the test. For applications that demand long-term stability in high-temperature environments, NiO_2:Cu and NiO_2:Mg serve as promising HTLs.

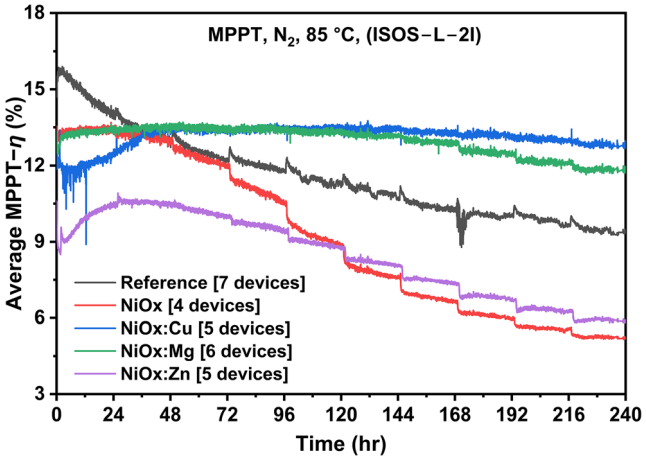

Figure 5. Averages of maximum power point tracking–η of the variously doped PSCs under the operational stability test (ISOS − L − 2I). The spikes and step-like η loss noticed are due to the periodical J–V measurement.

3.3. ZnO_xN_y-Based Thin-Film Transistors

The topic of large area flat panel displays technologies is strongly related to the developed of active matrix arrays to drive either liquid crystal or organic light-emitting diode displays. Moving from voltage-driven liquid crystal display (LCD) to current driven light-emitting diode display (OLED) technology opened the field for high mobility amorphous metal oxide thin-film transistors[25] where indium gallium zinc oxide turned out to be the most feasible material for the oxide channel layer.[26] Regarding the electron mobility, promising results have also been obtained for ZnO_xN_y-based TFTs where mobility of 47 $cm–0^2/Vs$ is reported as prepared for films deposited on unheated substrates

Table 2. WDX analysis of selected samples.

Sample nr.	Specification Ar-N-O [sccm]	C (at.%)	Zn (at.%)	N (at.%)	O (at.%)	Ar (at.%)
T1	1000-80-6	1.61	55.12	19.36	23.52	0.36
T4	1200-80-4	1.43	51.25	23.29	21.80	2.20

Table 1. Series of ZnO_xN_y based transistors as deposited.

Sample nr.	Ar. Flow [sccm]	N_2 Flow [sccm]	O_2 Flow [sccm]	Power [W]	ρ [Ωcm]	Carrier Conc. [cm^{-3}]	μ [cm^2/Vs]
T1	1000	80	6	300	1.49 E-1	–1.15 E + 18	36.3
T2	1000	80	6	300	2.18 E-1	–8.21 E + 17	34.9
T3	1000	80	8	300	1.56	–2-23 E + 17	18
T4	1200	80	4	250	2.88 E-2	–3.56 E + 18	60.7
T5	1200	80	6	250	1.03 E-1	–1.76 E + 18	34.3
T6	1200	80	8	250	3.74	-1.97 E + 17	8.44
T7	800	140	10	250	4.68	–1.57 E + 17	8.51

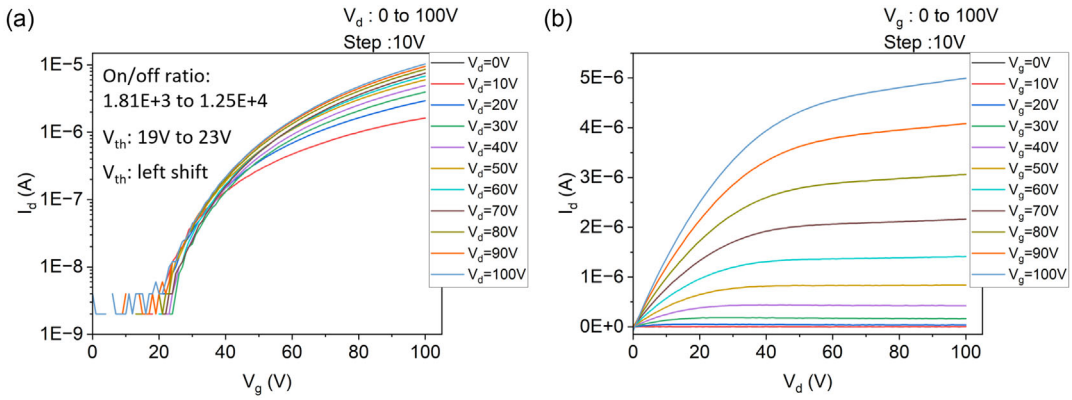

Figure 6. Sample T1 with 60 µm channel length–annealed @300 °C for 40 mins a) TFC b) OPC.

by reactive direct current (DC) magnetron sputtering compared to mobility of 110 $cm^2 Vs^{-1}$ after annealing at 400 °C.[27]

To investigate the performance of ZnOxNy-based TFTs, we prepared a set of samples deposited at different gas flow under standard conditions.[28]

The elemental composition has been measured by wavelength disperse X-ray spectroscopy (WDX). **Table 1** and **2** show the results for films with most attractive transistor characteristics, where the transfer and output characteristics (transfer characteristic (TFC) and output characteristic (OPC)) for sample T1 are shown in **Figure 6**.

TFTs with channel length of 60 µm showed the best on/off ratio in the order of 10^4, opening the door for the application in analog devices. Metal layer must be deposited through pulsed DC mode. The metal layer deposited through DC mode exhibits a huge gate leakage current. Annealing for short time like 30–40 mins does not degrade device performance. Annealing for longer time degrades device performance heavily.

These promising TFT results open the pathway for further device development. Our current interest is in TFT arrays on flexible substrates, where a transition from staggered bottom gate design toward the coplanar top gate design is necessary, where the dielectric for TFT is subject of optimization.

4. Summary and Outlook

In the last decade, substantial breakthroughs have been achieved in the area of hollow cathode GFS. Here, we have shown competitive performances for two important examples, NiO_x-based hole conductors in PSCs and for metal oxynitride films for TFTs. Further development will focus in both directions, currently the synthesis of SAM/NiO_x bilayers is subject of research as well as the development of dielectrics for TFTs in coplanar geometry to be used on flexible substrates. A further pathway for TCO development is toward the epitaxial growth of SnO_2 bases TCOs[29] taking advantage of the high plasma density in GFS to stimulate surface diffusion.

Acknowledgements

The authors acknowledge the financial support by the German Federal Ministry for Economic Affairs and Energy (BMWi) under contract number 0324095H (speedCIGS). The authors are grateful to S.A. (Helmholtz-Zentrum Berlin für Materialien und Energie) and the Helmholtz Innovation Lab HySPRINT for the PSC fabrication infrastructure. The authors express their gratitude to Natalia Maticiuc and Iver Lauermann for their support in PSC fabrication, as well as to Hans Köbler and Antonio Abate for supporting with the operational stability tests.

Open Access funding enabled and organized by Projekt DEAL.

Conflict of Interest

The authors declare no conflict of interest.

Author Contributions

Bernd Szyszka: project administration (lead); resources (lead); writing—original draft (lead). **Sri Hari Bharath Vinoth Kumar**: investigation (equal); writing—review & editing (supporting). **Ruslan Muydinov**: writing—review & editing (supporting). **Manuel Hartig**: investigation (equal); writing—review & editing (supporting). **Nivin Alktash**: investigation (equal); writing—review & editing (supporting). **Fangfang Huo**: investigation (equal); writing—review & editing (supporting). **Bertwin Bilgrim Otto Seibertz**: investigation (equal); writing—review & editing (supporting). **Nisarg Nijanandi**: investigation (equal); writing—review & editing (supporting). **Kai Ortner**: conceptualization (equal); methodology (equal); writing—review & editing (supporting). **Dennis Barton**: investigation (equal); methodology (equal); software (lead). **Steve Albrecht**: methodology (equal); supervision (equal).

Data Availability Statement

The data that support the findings of this study are available from the corresponding author upon reasonable request.

Keywords

NiO_x, perovskite solar cells, thin-film transistors, ZnO_xN_y

Received: February 25, 2025
Revised: April 2, 2025
Published online: May 15, 2025

[1] G. Bräuer, B. Szyszka, M. Vergöhl, R. Bandorf, *Vacuum* **2010**, *84*, 1354.

[2] H. J. Gläser, B. Szyszka, History of Glass Coating for Architectural Glazing, SVC TechConf. **2007**, *50*, 216–229.
[3] S. Ishibashi, Y. Higuchi, H. Nakamura, T. Komatsu, Y. Ota, K. Nakamura, Proc. ISSP **1991**, *1*, 153–158.
[4] N. Malkomes, A. Pflug, B. Szyszka, M. Vergöhl, SVC TechCon **2002**, *45*, 41–46.
[5] R. E. Somekh, *J. Vac. Sci. Technol. A* **1984**, *2*, 1285.
[6] K. Ishii, *J. Vac. Sci. Technol. A* **1989**, *7*, 256.
[7] T. Jung, A. Westphal, *Mater. Sci. Eng. B* **1991**, *140*, 528.
[8] M. Höfer, T. Jung, A. Jung, H. U. Kricheldorf, F. Schmidt, *SVC TechConf.* **2000**, *43*, 287–292
[9] H. Takeda, Y. Sato, Y. Iwabuchi, M. Yoshikawa, Y. Shigesato, *Thin Solid Films* **2009**, *517*, 3048.
[10] B. Szyszka, P. Löbmann, A. Georg, C. May, C. Elsässer, *Thin Solid Films* **2010**, *518*, 3109.
[11] Y. Kubo, Y. Iwabuchi, M. Yoshikawa, Y. Sato, Y. Shigesato, *J. Vac. Sci. Technol. A* **2008**, *26*, 893.
[12] N. Oka, A. Murata, S. Nakamura, J. Jia, J. Iwabuchi, H. Kotsubo, Y. Shigesato, *APL Mater.* **2015**, *3*, 104407.
[13] G. Pribil, Z. Hubicka, R. J. Soukup, N. J. Ianno, *J. Vac. Sci. Technol. A* **2001**, *19*, 1571.
[14] M. Birkholz, U. Albers, T. Jung, *Surf. Coat. Technol.* **2004**, *179*, 279.
[15] N. Alktash, R. Muydinov, D. Erfurt, M. Hartig, W. Gajewski, B. Szyszka, *Rev. Sci. Instrum.* **2023** *94*.
[16] A. Al-Ashouri, A. Magomedov, M. Roß, M. Jošt, M. Talaikis, G. Chistiakova, T. Bertram, J. A. Márquez, E. Köhnen, E. Kasparavičius, S. Levcenco, L. Gil-Escrig, C. J. Hages, R. Schlatmann, B. Rech, T. Malinauskas, T. Unold, C. A. Kaufmann, L. Korte, G. Niaura, V. Getautis, S. Albrecht, *Energy Environ. Sci.* **2019**, *12*, 3356.
[17] N. Alktash, S. Körner, T. Liu, A. Pflug, B. Szyszka, B., R. Muydinov, *Coatings* **2024**, *14*, 279.
[18] S. Liu, V. P. Biju, Y. Qi, W. Chen, Z. Liu, *NPG Asia Mater.* **2023**, *15*, 27.
[19] A. Magomedov, A. Al-Ashouri, A. E. Kasparavicius, S. Strazdaite, G. Niaura, M. Jost, T. Malinauskas, S. Albrecht, Y. Getautis, *Adv. Energy Mater.* **2018**, *8*.
[20] Y. Wang, R. Wenisch, R. Schlatmann, I. Lauermann, *Adv. Energy Mater.* **2018**, *8*.
[21] S. H. B. Vinoth Kumar, R. Muydinov, N. Maticiuc, N. Alktash, M. Rusu, B. B. O. Seibertz, H. Köbler, A. Abate, T. Unold, I. Lauermann, B. Szyszka, *Adv. Energy Sustain. Res.* **2023**, *5*.
[22] T. Yamazaki, K. Shigematsu, Y. Hirose, S. Nakao, I. Harayama, D. Sekiba, T. Hasegawa, *Appl. Phys. Lett.* **2016**, *109*.
[23] H. Köbler, S. Neubert, M. Jankovec, B. Glazar, M. Haase, C. Hilbert, M. Topic, B. Rech, A. Abate, *Energy Technol.* **2022**, *10*.
[24] M. V. Khenkin, E. A. Katz, A. Abate, G. Bardizza, J. J. Berry, C. Brabec, F. Brunetti, V. Bulovic, Q. Burlingame, A. Di Carlo, R. Cheacharoen, Y. B. Cheng, A. Colsmann, S. Cros, K. Domanski, M. Dusza, C. J. Fell, S. R. Forrest, Y. Galagan, D. Di Girolamo, M. Grätzel, A. Hagfeldt, E. von Hauff, H. Hoppe, J. Kettle, H. Köbler, M. S. Leite, S. Liu, Y. L. Loo, J. M. Luther, et al., *Nat. Energy* **2020**, *5*, 35.
[25] J. F. Wager, *Inf. Disp.* **2014**, *2*, 26.
[26] T. Kamiya, K. Nomura, H. Hosono, *Sci. Technol. Adv. Mater.* **2010**, *11*, 044305.
[27] Y. Ye, R. Lim, J. M. White, *J. Appl. Phys.* **2009**, *106*.
[28] N. Nijanandi, *Master Thesis,* TU Berlin **2023**.
[29] F. Huo, R. Muydinov, B. B. O. Seibertz, C. Wang, M. Hartig, N. Alktash, P. Gao, B. Szyszka, *Heliyon* **2024**, *10*, e30943.